FREQUENCY DOMAIN IDENTIFICATION OF GRINDING STIFFNESS AND DAMPING

Marco Leonesio[a], Paolo Parenti[b], Giacomo Bianchi[a]

[a]CNR — Institute of Industrial Technology and Automation, via Bassini 15, Milan, Italy

[b]Department of Mechanical Engineering, Politecnico di Milano, via La Masa 1, Milan, Italy

Corresponding author e-mail: marco.leonesio@itia.cnr.it (M. Leonesio)

other email-addresses: paolo.parenti@polimi.it (P. Parenti), giacomo.bianchi@itia.cnr.it (G. Bianchi).

Abstract

As equivalent stiffness and damping of the grinding process dominate cutting stability, their identification is essential to predict and avoid detrimental chatter occurrence. The identification of these process constants is not easy in large cylindrical grinding machines, e.g. roll grinders, since there are no practical ways to measure cutting force normal component. This paper presents a novel frequency domain approach for identifying these process parameters, exploiting in-process system response, measured via impact testing. This method adopts a sub-structuring approach to couple the wheel-workpiece relative dynamic compliance with a two-dimensional grinding force model that entails both normal and tangential directions. The grinding specific energy and normal force ratio, that determine grinding stiffness and damping, are identified by fitting the closed loop FRF (Frequency Response Function) measured during specific plunge-grinding tests. The fitting quality supports the predictive capability of the model. Eventually, the soundness of the proposed identification procedure is further assessed by comparing the grinding specific energy identified through standard cutting power measurements.

Keywords: grinding; force model identification; dynamic sub-structuring; frequency domain.

NOMENCLATURE (Symbols and Abbreviations)

a [mm]	actual infeed	k_t [N/mm^2]	grinding specific energy
b [mm]	grinding (cutting) width	k_n [N/mm^2]	normal force coefficient
$\mathbf{C}(\omega_j)$ [mm^3/N^2]	matrix associated to the coefficient identification	$\mathbf{K}_g$ [N/mm], $\mathbf{K}_{gd}$ [N·s/mm]	grinding stiffness and grinding damping matrices
$\mathbf{c}_n(\omega_j)$ [mm^3/N^2]	column of $\mathbf{C}(\omega_j)$ associated to k_n	LS	Least Squares
$\mathbf{c}_t(\omega_j)$ [mm^3/N^2]	column of $\mathbf{C}(\omega_j)$ associated to k_t	LVDT	Linear Variable Differential Transformer

δt, δn [mm] $\dot{\delta t}$, $\dot{\delta n}$ [mm/s]	small perturbations in tangent and normal direction	μ	ratio between normal and tangential force components
d [mm]	vector of displacements in normal and tangential direction	**M** [mm/N]	projected compliance matrix
D_{eq} [mm]	equivalent diameter	$m_{...}$ [mm/N]	elements of projected compliance matrix **M**
D_r [mm]	roll diameter	MIMO	Multi Input Multi Output
D_w [mm]	wheel diameter	MRR_0 [mm^2/s]	material removal rate in the static case normalized with respect to grinding width
DoF	Degree of Freedom	MRR [mm^2/s]	Material Removal Rate normalized with respect to grinding width
FEM	Finite Element Method	P	set of process DoFs
F_n [N]	normal grinding force	P_{s0} [W]	spindle power without material removal
F_t [N]	tangential grinding force	P_s [W]	overall spindle motor output power
FRF	Frequency Response Function	ω [1/s]	pulsation
H [mm/N]	overall compliance matrix of full system dynamics	*rn, rt, wn, wt*	DoFs components for roll (*r*), wheel (*w*) in normal (*n*) and tangential direction (*t*)
$h_{BA_{CL}}$ [mm/N]	closed-loop FRF identified by measurements	σ	semi-interval of the identified parameters
$\mathbf{h}^T_{BP}$ [mm/N]	FRFs vector relating input forces at process DoFs to the displacement at the additional output DoF B;	sgn Ω	sign of wheel velocity
$\mathbf{h}_{PA}$ [mm/N]	FRFs vector relating a force at the additional input DoF A to the output displacements at the process DoFs;	$\mathbf{t}(\omega_j)$ [mm/N]	known terms vector of the identification system
h_{wn_wn} [mm/N]	static compliance	V_W, V_S [m/s]	wheel and roll velocities

1. Introduction

In grinding, multiple abrasive particles of the grinding wheel — with different size, distribution and orientation — act together to produce a complex and stochastic grinding force signature [1]. Several force models, ranging from physical to empirical/statistical, have been proposed in grinding literature, as reported in this exhaustive survey from CIRP [2]. Despite generality of physical approaches is theoretically broader, mixed analytical-empirical models are mostly used, thanks to their easy calibration in real cases with simple experimental setups.

Different formulations have been proposed over the years for improving modelling accuracy: those based on specific energy concept [3] are the simplest and most used to cope with force estimation and cutting stability issues.

Cylindrical grinding stability is usually strictly related to normal — i.e. radial — dynamic compliance between wheel and roll. For this reason, grinding dynamics is often studied reducing system behavior to the solely normal direction [4]. Normal force component does not generate cutting power but just a load on machine structure that provokes a relative displacement between wheel and workpiece. In regenerative chatter stability analysis the cutting process is typically described by means of a "grinding stiffness" (or "cutting stiffness"), i.e. the ratio between normal grinding force and actual infeed [5], and a "grinding damping", relating force to vibrational velocity in normal direction.

A two DoFs (degrees of freedom) process model — that considers also the tangential force component and the corresponding displacement — has been proposed in [6] to deal with cutting instability generated by damping forces acting on vibration modes involving both radial and tangent displacements. Then, an additional coefficient is needed: the ratio between normal and tangential force components.

Relying on this 2D model, this paper characterizes the coupled machine-process behavior in the frequency domain and performs a reverse identification of grinding stiffness, grinding damping and normal/tangential ratio by a sub-structuring method. The adopted approach is the well known RCSA method (Receptance Coupling Substructure Analysis) that predicts frequency responses of a specific system, combining its substructures responses [7]-[12]. Schmitz and Donalson [7] were the first to propose RCSA for tool-tip FRF identification. Park et al. [8] presented an improved receptance coupling technique for the same purpose: the end mill was modeled numerically as a cylindrical beam, and spindle-tool-holder system FRF was identified by means of impact testing on two different blank cylinders — used as calibration tools — clamped on the tool-holder. Calibration tools were adopted to determine rotational responses using IRCSA (Inverse RCSA), by conducting additional experiments. In general, several authors adopt IRCSA to solve the reverse problem of joint identification between two substructures [13]-[15]. However, in all these works, the joint is modeled as a pure mechanical impedance, namely, a "joint dynamic stiffness matrix" [14]. Conversely, in the present study, the "joint" is represented by the grinding process. The grinding process exerts a force that depends on relative displacements and velocities of the connection points but, basing on the developed physical process model, a specific structure of the two by two stiffness and damping matrices is assumed, reducing the number of parameters to be identified down to two real unknowns. For this reason, the proposed mathematical elaboration is basically new in the literature and allows an easy characterization of the cutting dynamic behavior of medium/large cylindrical grinders — such as traverse/roll grinders — without making use of direct cutting force measurements.

Excitation of closed-loop process dynamics was implemented in [16], where an electro-dynamic shaker and a bearing connection were used to excite the workpiece during the grinding process. The aim of the authors was to test the effect of a random excitation on chatter occurrence but no cutting parameter identification was performed. In a similar way, in [17] workpiece dynamic compliance was measured in open and closed loop

conditions — during a plunge grinding operations. The authors found a significant difference in the resonance peaks for the two situations and they explained it as a mere closure of the mechanical loop originated by the mechanical contact between wheel and workpiece. Indeed, as the following paragraph will explain, they likely saw the effects of dynamic coupling produced by grinding force field, coupled to system states, i.e. relative position and velocity. For sake of clarity, some misleading statements are worth to by cited: "The stiffness increase is probably from the extra support of the wheel to the flexible workpiece, i.e., a change of boundary condition, while the damping increase […] is possibly due to the porous structure of the vitrified grinding". As shown in the present work, the closed loop analysis should consider the force field produced by the grinding process as a dynamic coupling between the mechanical elements constituted by the grinding wheel and the workpiece.

Grinding stiffness and its coupling with machine dynamic stiffness have a predominant effect on system stability. In [18] grinding tests with variable workpiece dynamics were executed and compared to numerical simulations, in predicting cutting stability. In this scenario, process constants identification is important and can also support advanced schemes for wheel and workpiece waviness monitoring during chatter onset [19].

Identification of grinding force models usually requires measurement of grinding power/forces and actual material removal. Specific energy is estimated relating the grinding power — which is the product of tangential cutting force and cutting speed — to the specific material removal rate (*MRR*). In most of the literature, specific energy increases with a decreasing radial infeed, that reduces the equivalent chip thickness. Several researchers explain this phenomenon through the so-called "size-effect", related to the ploughing power component, and assume a constant ploughing force per contact width ratio. Conversely, sliding power is usually modeled as proportional to wear flats area on wheel surface [20]. Whereas these two latter components exist even without material shear and chip formation, their importance decreases as chip thickness increases, generating a process non-linearity, associated with the transition of the removal mechanism from plowing to chip formation [21].

Simplified methodologies to determine cutting stiffness in plunge grinding were presented in [22] and [23]: they were based on the identification of the structural elastic recovery time constant, which defines the exponential decay of actual infeed after an initial nominal infeed. This methodology entails the knowledge of wheel-workpiece relative stiffness, whose identification requires accurate force/displacement measurements. In this works, force measurement systems based on displacement sensors were adopted: a LVDT transducer mounted at workpiece headstock [22], and a capacitive sensor embedded in work spindle [23]. Direct cutting force measurement is simple in surface grinding machines by installing a dynamometric table onto the machine table [24]. However, both these solutions become complex and not suitable in case of medium/large industrial roll grinders: sensors placement might foresee machine components reworking — e.g., sensors embedded in the spindle — while external solutions could imply the design of large auxiliary structures for sensor support.

An experimental procedure that does not requires cutting force measurements for evaluating grinding stiffness in cylindrical grinding has been patented in recent years [25]. It is based on spiral grinding tests and on spiral marks measurements on the workpiece (width and depth). All these methods require the knowledge of machine

structural stiffness — therefore prescribing a static compliance measure — and neglect grinding process damping — which indeed is necessary to predict chatter occurrence [4].

Moreover, grinding system behavior changes along production time because of wheel wear, change in workpiece mass, lubrication condition, etc. Being able to estimate in real-time grinding constants is another paradigm that was addressed [26], which provides a real-time estimation of grinding process parameters through recursive identifications (Extended Kalman Filter and least-squares), hinged at model-based control of grinding dynamics. Again, this approach requires experiments involving direct/indirect force measurements through force sensors (strain-gauge and piezoelectric type) and radial displacement sensor (eddy current probe).

Those remarks and the above mentioned scientific/industrial needs motivate the present paper, aiming at identifying a grinding process force model that is inherently suited to stability study in medium/large cylindrical grinding machines, without requiring force and displacement measurements.

The paper is structured as follows. First, grinding force model is presented, together with its interaction with system dynamics; then, equations for process parameters identification, starting from out-of-process and in-process dynamic compliances, are introduced. Then, a section describes tap testing setup for measuring the in-process FRF. Eventually, specific energy identification trough FRFs is compared to identification based on classical power measurements during grinding tests. Discussion and conclusions complete the article.

2. Methodology description

The identification of a 2D grinding force model, able to reproduce process excitations in both normal and tangential directions, is herewith proposed to analyze machine-process dynamic interaction in roll grinding. The adopted model is based on a minimal set of parameters: specific energy and grinding stiffness. Parameters identification is performed without requiring force measurements during grinding tests, but considering how process forces affect machine dynamics.

Coupling process model with machine dynamics, it is possible to predict how the dynamic compliance measured at rest (i.e. *out-of-process*) changes during grinding (i.e. *in-process*). Dually, this difference can be exploited to identify the two process parameters. Considering the reduced number of parameters, a good matching between predicted and experimental in-process dynamic compliance (for a significant frequency range) is not trivial and demonstrates by itself the validity of the model.

A substructuring technique is adopted to predict the effect of process forces on machine dynamics, in particular on workpiece dynamic compliance in normal direction (the FRF selected for the identification, see par. 5.3).

The process model applies forces to the out-of-process wheel-workpiece relative dynamics: the resulting oscillations, in turn, affect the actual infeed. This dependency closes a dynamic loop through the process: for this reason, the out-of-process FRFs are also indicated as *open-loop FRFs*, while the in-process FRFs become *closed-loop FRFs*.

The closed-loop FRFs more suited for the identification are those mostly influenced by the process. In this study, a single closed-loop FRF has been used: the dynamic compliance at workpiece (namely, *roll* or *cylinder*) in normal direction.

The methodology can be synthetized in the following steps:

- Development of the grinding force model;
- Determination of the equations for the machine-process closed loop dynamics and for parameters identification;
- Measurement of the dynamic compliances necessary to feed the identification system: wheel-workpiece in tangential and normal direction, roll side in normal direction open-loop, roll side in normal direction closed-loop;
- Parameters identification via Least Squares (LS) solution in a proper frequency range.

3. Machine-process dynamic interaction

3.1.Grinding process model

As recalled in the introduction, in most of the literature, the grinding power is assumed to be a monotonic function of the material removal rate (*MRR*). Then, the tangential grinding force F_t associated to that power can be determined knowing the wheel velocity, while the normal component F_n is usually considered proportional to the tangential one. These components are expressed with respect to a reference frame located at the ideal contact point between wheel and workpiece (see, in Figure 1, the grinding forces, applied to the wheel).

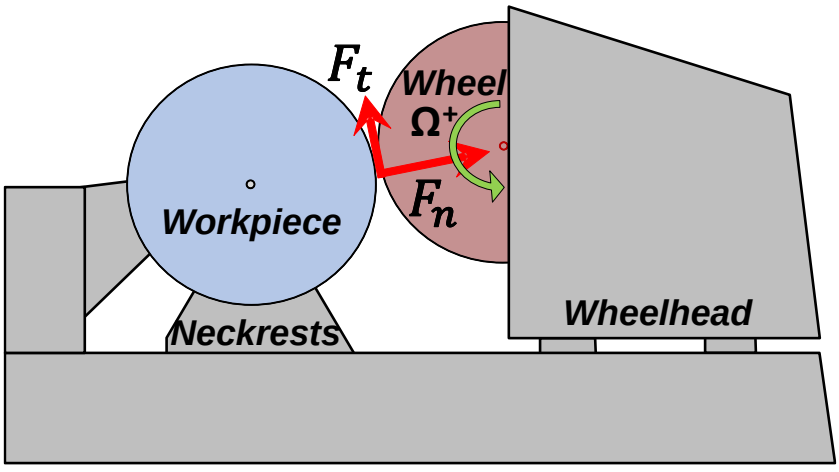

Figure 1. Grinding forces components

Based on these definitions, the following force model is considered, which can be generalized for any kind of wheel-workpiece engagement (see [27],[6]):

$$\begin{Bmatrix} F_t \\ F_n \end{Bmatrix} = bk_t \begin{Bmatrix} \operatorname{sgn}\Omega \\ \mu \end{Bmatrix} \left(\frac{MRR}{V_s} \right) \tag{1}$$

where:

- b: grinding width;
- k_t: specific energy associated to material removal;
- μ: ratio between normal and tangential force components;
- V_S: grinding velocity (that basically coincides with the wheel peripheral velocity);
- "sgn Ω": sign of wheel velocity (positive according to arrow in Figure 1);
- *MRR*: Material Removal Rate, normalized with respect to grinding width.

In the static case (namely, without vibrations), the *MRR* is given by the following expression:

$$MRR_0 = aV_w \tag{2}$$

where a is the actual infeed and V_w the workpiece velocity. A general expression for the *MRR* - taking into account also dynamic displacement components - can be obtained linearizing the expression of the material flow through the contact arc when wheel-workpiece relative position and velocity are subject to small perturbations in tangent and normal direction, denoted with δt, $\delta \dot{t}$, δn, $\delta \dot{n}$:

$$MRR \cong \left(V_w + \delta \dot{t}\right)\left(a + \delta n\right) + \delta \dot{n}\sqrt{aD_{eq}} = MRR_0 + a\delta \dot{t} + V_w \delta n + \delta \dot{n}\sqrt{aD_{eq}} \tag{3}$$

where D_{eq} is the equivalent diameter given by $D_wD_r/(\mathrm{D}_w+\mathrm{D}_r)$, with D_w and D_r wheel and roll diameters respectively.

Finally, Eq.(3) can be substituted into Eq.(1) to express force perturbation around the equilibrium:

$$\begin{aligned} &\begin{Bmatrix} \delta F_t \\ \delta F_n \end{Bmatrix} = bk_t \begin{Bmatrix} \operatorname{sgn}\Omega \\ \mu \end{Bmatrix} \cdot \left(\frac{a\delta \dot{t} + V_w \delta n + \delta \dot{n}\sqrt{aD_w}}{V_s} \right) = \\ &= \frac{bk_t}{V_s} \left(\begin{bmatrix} a\operatorname{sgn}\Omega & \operatorname{sgn}\Omega\sqrt{aD_{eq}} \\ \mu a & \mu\sqrt{aD_{eq}} \end{bmatrix} \begin{Bmatrix} \delta \dot{t} \\ \delta \dot{n} \end{Bmatrix} + V_w \begin{bmatrix} 0 & \operatorname{sgn}\Omega \\ 0 & \mu \end{bmatrix} \begin{Bmatrix} \delta t \\ \delta n \end{Bmatrix} \right) \end{aligned} \tag{4}$$

Let the following equivalent grinding stiffness and damping matrices be defined:

$$\mathbf{K}_g \overset{def}{=} \frac{bk_t V_w}{V_s}\begin{bmatrix} 0 & \operatorname{sgn}\Omega \\ 0 & \mu \end{bmatrix}; \qquad \mathbf{K}_{gd} \overset{def}{=} \frac{bk_t}{V_s}\begin{bmatrix} a\operatorname{sgn}\Omega & \operatorname{sgn}\Omega\sqrt{aD_{eq}} \\ \mu a & \mu\sqrt{aD_{eq}} \end{bmatrix} \tag{5}$$

Then Eq.(4) can be rewritten as follows:

$$\begin{Bmatrix} \delta F_t \\ \delta F_n \end{Bmatrix} = \mathbf{K}_{gd}\begin{Bmatrix} \delta \dot{t} \\ \delta \dot{n} \end{Bmatrix} + \mathbf{K}_g \begin{Bmatrix} \delta t \\ \delta n \end{Bmatrix} \tag{6}$$

Since the identification methodology encompasses the in-process measurement of roll dynamics via tap testing, the grinding operation considered for the experiment must exhibit a stable behavior. This assumption entails the possibility to neglect, in the determination of the actual infeed, wheel and workpiece regeneration loops, which are modeled by many authors to explain the origin of grinding chatter [4]. Therefore, the proposed model does not consider any time delay: only the current instantaneous value of the states is supposed to affect grinding forces.

3.2. Machine model

The machine model must describe wheel and cylinder relative dynamics, providing the relative displacements/velocities involved in the grinding forces expression, i.e. Eq.(4). Wheel/workpiece dynamic behavior is usually rather linear and can be represented by a set of FRFs displacement over force. The grinding force acts on both wheel and cylinder, both in tangential and normal direction, while being influenced by the relative displacement along the same directions. Thus, the minimal dynamics to be described for studying the grinding process is represented by a MIMO system defined by a 4x4 compliance matrix (for sake of compactness the dependence on frequency is hidden):

$$\mathbf{H}_{pp} \overset{def}{=} \begin{bmatrix} h_{wt\_wt} & h_{wt\_wn} & h_{wt\_rt} & h_{wt\_rn} \\ h_{wn\_wt} & h_{wn\_wn} & h_{wn\_rt} & h_{wn\_rn} \\ h_{rt\_wt} & h_{rt\_wn} & h_{rt\_rt} & h_{rt\_rn} \\ h_{rn\_wt} & h_{rn\_wn} & h_{rn\_rt} & h_{rn\_rn} \end{bmatrix} \tag{7}$$

where subscript "*w*" stays for "*wheel side*", "*r*" for "*roll side*", "*t*" for "*tangential direction*" and "*n*" for "*normal direction*", while "*P"* indicates the set of the above-mentioned DoFs (*process DoFs*): $P=\{p_1, p_2, p_3, p_4\}=\{$"wt", "wn", "rt", "rn"$\}$.

For the closed-loop FRF required by the identification system any other DoF of the machine can be used. Once defined such additional input/output DoF pair (*A*,*B*), which can even coincide with one of the process DoF, the overall compliance matrix describing the full system dynamics is defined as follows:

$$\mathbf{H} \overset{def}{=} \begin{bmatrix} \mathbf{H}_{PP} & \mathbf{h}_{PA} \\ \mathbf{h}^{T}_{BP} & h_{BA} \end{bmatrix} \tag{8}$$

where

- $\mathbf{h}_{PA\,(5x1)}$ is the FRFs vector relating a force at the additional input DoF *A* to the displacements at the process DoFs;
- $\mathbf{h}^{T}_{BP\,(1x5)}$ is the FRFs vector relating input forces at process DoFs to the displacement at the additional output DoF *B*;
- h_{BA} is the FRF relating a force at the additional input DoF *A* to the displacement at the additional output DoF *B*.

The elements of matrix **H** are identified experimentally via tap testing procedure, as described in par. 4.

3.3. Coupled model

The dynamic coupling between machine and process was attained by connecting wheel-workpiece relative dynamics with the grinding forces that depends on wheel-workpiece relative displacements. This connection corresponds to a structural modification that realizes a closed loop in the structure: coherently with the treatment exposed in par. 3.1 — namely, Eq. (4) — this load is given by the dynamic component of grinding force associated to nominal process parameters. Substructuring techniques can be profitably exploited to carry out such a structural modification [28].

The diagram of Figure 2 represents such a coupling, where the input are wheel-workpiece relative nominal displacements in tangential (usually null) and normal directions (radial infeed).

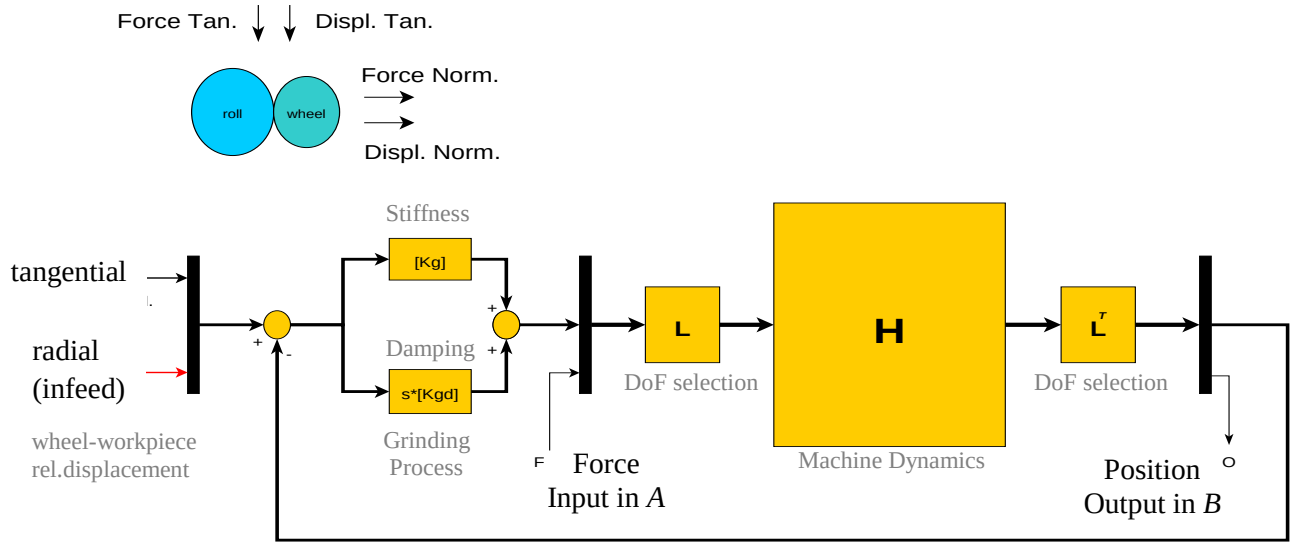

Figure 2. Dynamic model of grinding process

The incident matrix **L** appearing in the scheme generates two opposite grinding forces — for both normal and tangential components — on wheel and roll, and the input force *F*, which is the excitation for the closed-loop impact testing, on the selected DoF *A*:

$$\mathbf{L} \overset{def}{=} \begin{bmatrix} 1 & 0 & 0 \\ 0 & 1 & 0 \\ -1 & 0 & 0 \\ 0 & -1 & 0 \\ 0 & 0 & 1 \end{bmatrix} \tag{9}$$

On the other side, $\mathbf{L}^T$ provides the summation of wheel and roll responses in tangential and normal directions in order to get the relative displacement; moreover, the further row produces *B* DoF displacement (denoted with the variable *O*), that is the output of the closed-loop impact testing.

Now, let **d** be the vector of displacements in normal and tangential direction, namely:

$$\mathbf{d} \overset{def}{=} \begin{Bmatrix} \delta t \\ \delta n \end{Bmatrix} \tag{10}$$

Then, the closed-loop equation of dynamic equilibrium can be written:

$$\mathbf{L}^T \mathbf{H} \mathbf{L} \left(\begin{Bmatrix} \mathbf{0} \\ F \end{Bmatrix} - \begin{bmatrix} 1 & 0 \\ 0 & 1 \\ 0 & 0 \end{bmatrix} \left(\mathbf{K}_g + s\mathbf{K}_{gd} \right) \mathbf{d} \right) = \begin{Bmatrix} \mathbf{d} \\ O \end{Bmatrix} \tag{11}$$

Let matrix **M** and its partition be defined as follows:

$$\mathbf{M} \overset{def}{=} \begin{bmatrix} m_{tt} & m_{tn} & m_{tA} \\ m_{nt} & m_{nn} & m_{nA} \\ m_{Bt} & m_{Bn} & m_{BA} \end{bmatrix} \overset{def}{=} \mathbf{L}^T \mathbf{H} \mathbf{L} = \begin{bmatrix} \begin{pmatrix} h_{wt\_wt} - h_{wt\_rt} + \\ -h_{rt\_wt} + h_{rt\_rt} \end{pmatrix} & \begin{pmatrix} h_{wt\_wn} - h_{wt\_rn} + \\ -h_{rt\_wn} + h_{rt\_rn} \end{pmatrix} & \left(h_{wt\_A} - h_{rt\_A} \right) \\ \begin{pmatrix} h_{wn\_wt} - h_{wn\_rt} + \\ -h_{rn\_wt} + h_{rn\_rt} \end{pmatrix} & \begin{pmatrix} h_{wn\_wn} - h_{wn\_rn} + \\ -h_{rn\_wn} + h_{rn\_rn} \end{pmatrix} & \left(h_{wn\_A} - h_{rn\_A} \right) \\ \left(h_{B\_wt} - h_{B\_rt} \right) & \left(h_{B\_wn} - h_{B\_rn} \right) & h_{BA} \end{bmatrix} \tag{12}$$

Then, Eq.(11) can be solved, after substituting **M**, w.r.t. the closed-loop FRF, that is the ratio *O*/*F*:

$$\begin{cases} -\begin{bmatrix} m_{tt} & m_{tn} \\ m_{nt} & m_{nn} \end{bmatrix} \left(\mathbf{K}_g + s\mathbf{K}_{gd} \right) \mathbf{d} + \begin{Bmatrix} m_{tA} \\ m_{nA} \end{Bmatrix} F = \mathbf{d} \;\Rightarrow\; \mathbf{d} = \left(\begin{bmatrix} m_{tt} & m_{tn} \\ m_{nt} & m_{nn} \end{bmatrix} \left(\mathbf{K}_g + s\mathbf{K}_{gd} \right) + \mathbf{I} \right)^{-1} \begin{Bmatrix} m_{tA} \\ m_{nA} \end{Bmatrix} F \\ m_{BA} F - \{ m_{Bt} \quad m_{Bn} \} \left(\mathbf{K}_g + s\mathbf{K}_{gd} \right) \mathbf{d} = O \end{cases}$$

$$\Rightarrow m_{BA} F - \{ m_{Bt} \quad m_{Bn} \} \left(\mathbf{K}_g + s\mathbf{K}_{gd} \right) \left(\begin{bmatrix} m_{tt} & m_{tn} \\ m_{nt} & m_{nn} \end{bmatrix} \left(\mathbf{K}_g + s\mathbf{K}_{gd} \right) + \mathbf{I} \right)^{-1} \begin{Bmatrix} m_{tA} \\ m_{nA} \end{Bmatrix} F = O \tag{13}$$

$$\Rightarrow h_{BA_{CL}} \overset{def}{=} \frac{O}{F} = m_{BA} - \{ m_{Bt} \quad m_{Bn} \} \left(\begin{bmatrix} m_{tt} & m_{tn} \\ m_{nt} & m_{nn} \end{bmatrix} + \left(\mathbf{K}_g + s\mathbf{K}_{gd} \right)^{-1} \right)^{-1} \begin{Bmatrix} m_{tA} \\ m_{nA} \end{Bmatrix}$$

Since $\mathbf{K}_g = \mathbf{K}_g \left(k_t, \mu \right)$ and $\mathbf{K}_{gd} = \mathbf{K}_{gd} \left(k_t, \mu \right)$, then $h_{BA_{CL}} = h_{BA_{CL}} \left(k_t, \mu \right)$. Thus k_t and μ can be obtained solving the following functional equation:

$$h_{BA_{CL}} \left(k_t, \mu \right) = h_{BA_{CL}\, mea} \tag{14}$$

where $h_{BA_{CL}\, mea}$ is the closed-loop FRF identified by measurements (see par. 4.2).

Posing $k_n \overset{def}{=} \mu k_t$, Eq.(14) becomes linear in the unknowns k_t and k_n. Substituting the expressions of $\mathbf{K}_g$ and $\mathbf{K}_{gd}$ (obtained in par 3.1) into $h_{BA_{CL}}$, the identification equation can be made explicit as follows:

$$\begin{aligned} &\left(\left(\left(\sqrt{aD_{eq}} m_{nn} + m_{tn} a \right) h_{BA_{CL}} - \left(\sqrt{aD_{eq}} m_{nn} + M_{tn} a \right) m_{BA} + m_{Bn} \left(\sqrt{aD_{eq}} m_{nA} + m_{tA} a \right) \right) i\omega + \right. \\ &\left. + \left(h_{BA_{CL}} m_{nn} - m_{BA} m_{nn} + m_{nA} m_{Bn} \right) V_w \right) \frac{b}{V_s} k_n + \\ &\left(\left(\left(\sqrt{aD_{eq}} m_{nt} + m_{tt} a \right) h_{BA_{CL}} - \left(\sqrt{aD_{eq}} m_{nt} + m_{tt} a \right) m_{BA} + m_{Bt} \left(\sqrt{aD_{eq}} m_{nA} + m_{tA} a \right) \right) i\omega + \right. \\ &\left. + \left(h_{BA_{CL}} m_{nt} - m_{BA} m_{nt} + m_{tA} m_{Bt} \right) V_w \right) \frac{b}{V_s} k_t \operatorname{sgn} \Omega + \\ &+ h_{BA_{CL}} - m_{BA} = 0 \end{aligned} \tag{15}$$

Eq.(15) entails a scalar equation for each value of frequency 'ω', that is the independent parameter of the transfer functions in matrix **M**.

Since the actual infeed is usually significantly smaller than the arc of contact between wheel and workpiece, it can be stated that $a << \sqrt{aD_w}$ and $\omega a << V_w$: i.e. all terms having the actual infeed as factor can be neglected. Additionally, we note that, if the dynamical behavior in tangent and normal direction is decoupled, implying $|m_{nt}|,|m_{tn}|,|m_{Bt}|,|m_{tA}| \cong 0$, Eq.(15) becomes:

$$\left(\left(m_{nn}h_{BA_{CL}} - m_{nn}m_{BA} + m_{Bn}m_{nA}\right)\sqrt{aD_{eq}}\,i\omega + \left(h_{BA_{CL}}m_{nn} - m_{BA}m_{nn}\right)V_w\right)\frac{b}{V_s}k_n + h_{BA_{CL}} - m_{BA} = 0 \tag{16}$$

and k_t becomes unidentifiable. Therefore, the full identification of process model can be attained only if dynamics in normal and tangential direction are someway coupled, by slanted vibration modes in the frequency range of interest.

3.4.Model parameters identification

Knowing the open loop FRFs, i.e. the elements of matrix **M**, Eq.(15) establishes a functional relationship between coefficients k_n and k_t and the "in-process" FRF relating force input *A* to displacement output *B*. This functional relationship can be sampled in a system of *N* equations by evaluating the dynamic compliances for *N* frequencies ω_j in a proper frequency range; then, the system can be solved for k_n and k_t.
Let the following vectors/matrix be defined:

$$\begin{aligned}
\mathbf{c}_n\left(\omega_j\right) &\overset{def}{=} \left\{\left(\begin{array}{l}\left(\sqrt{aD_{eq}}m_{nn}\left(\omega_j\right) + m_{tn}\left(\omega_j\right)a\right)h_{BA_{CL}} + \\ -\left(\sqrt{aD_{eq}}m_{nn}\left(\omega_j\right) + m_{tn}\left(\omega_j\right)a\right)m_{BA}\left(\omega_j\right) + \\ +m_{Bn}\left(\omega_j\right)\left(\sqrt{aD_{eq}}m_{nA}\left(\omega_j\right) + m_{tA}\left(\omega_j\right)a\right)\end{array}\right)i\omega_j + \right.\\
&\qquad \left. + \left(h_{BA_{CL}}m_{nn}\left(\omega_j\right) - m_{BA}\left(\omega_j\right)m_{nn}\left(\omega_j\right) + m_{nA}\left(\omega_j\right)m_{Bn}\right)\left(\omega_j\right)V_w\right)\frac{b}{V_s}\right\};\\
\mathbf{c}_t\left(\omega_j\right) &\overset{def}{=} \left\{\left(\begin{array}{l}\left(\sqrt{aD_{eq}}m_{nt}\left(\omega_j\right) + m_{tt}\left(\omega_j\right)a\right)h_{BA_{CL}} + \\ -\left(\sqrt{aD_{eq}}m_{nt}\left(\omega_j\right) + m_{tt}\left(\omega_j\right)a\right)m_{BA}\left(\omega_j\right) + \\ +m_{Bt}\left(\omega_j\right)\left(\sqrt{aD_{eq}}m_{nA}\left(\omega_j\right) + m_{tA}\left(\omega_j\right)a\right)\end{array}\right)i\omega_j + \right.\\
&\qquad \left. + \left(h_{BA_{CL}}\left(\omega_j\right)m_{nt}\left(\omega_j\right) - m_{BA}\left(\omega_j\right)m_{nt}\left(\omega_j\right) + m_{nA}\left(\omega_j\right)m_{Bt}\left(\omega_j\right)\right)V_w\right)\frac{b}{V_s}\operatorname{sgn}\Omega\right\};\\
\mathbf{C}\left(\omega_j\right) &\overset{def}{=} \left[\mathbf{c}_n\left(\omega_j\right) \quad \mathbf{c}_t\left(\omega_j\right)\right];\\
\mathbf{t}\left(\omega_j\right) &\overset{def}{=} \left\{m_{BA}\left(\omega_j\right) - h_{BA_{CL}}\left(\omega_j\right)\right\};
\end{aligned} \tag{17}$$

Then, Eq.(15) becomes:

$$\mathbf{C}\left(\omega_j\right)\begin{Bmatrix}k_n\\ k_t\end{Bmatrix} = \mathbf{t}\left(\omega_j\right) \tag{18}$$

As real values for k_n and k_t are wanted, being $\mathbf{C}(\omega_j)$ and $\mathbf{t}(\omega_j)$ complex numbers, Eq.(18) can be rewritten in real form as follows (as suggested in [14]):

$$\begin{bmatrix} \Re(\mathbf{C}(\omega_j)) \\ \Im(\mathbf{C}(\omega_j)) \end{bmatrix} \begin{Bmatrix} k_n \\ k_t \end{Bmatrix} = \begin{Bmatrix} \Re(\mathbf{t}(\omega_j)) \\ \Im(\mathbf{t}(\omega_j)) \end{Bmatrix} \tag{19}$$

Finally, Eq.(19) can be solved in the Least Squares sense.

4. Experimental campaign

An experimental campaign was conducted on a commercial middle-sized roll grinding machine, with a wheel spindle of 15 kW and maximum roll length of 3000 mm. Supplementary grinding tests with spindle power measurements were performed to identify k_t with the classical approach based on specific energy, to compare the result with the one obtained by the proposed approach.
The experimental campaign was structured as follows:

- Open-loop FRFs measurements at rest, via tap testing on wheel and cylinder;
- Selection of the best in-process measurement DoF *A* and *B*;
- Closed-loop FRFs measurements during a plunge grinding operation (in the same wheel position along the cylinder as for the open-loop FRFs measurement);
- Traverse grinding tests at different infeed, wheel and roll speed, with wheel spindle power measurements, for classic specific energy identification.

5. Results

5.1. Process identification from FRFs fitting

5.1.1. Open loop FRFs measurement

Open loop machine dynamics was characterized by impact testing measuring wheel and roll requires absolute compliances, with standard instrumented hammer and accelerometers, and computing the relative compliances, in both radial and tangential directions. Other DOFs can be added, for off-line and in-process measurements. In the present study, to minimize the experimental burden, the already mentioned wheel and roller DOFs were candidate also for in-process measurement.
The FRFs composing the compliance matrix **H** were measured with the setup illustrated in Figure 3. Machine axes controller were active during the open-loop FRFs measurement in order to better represent in-process conditions.

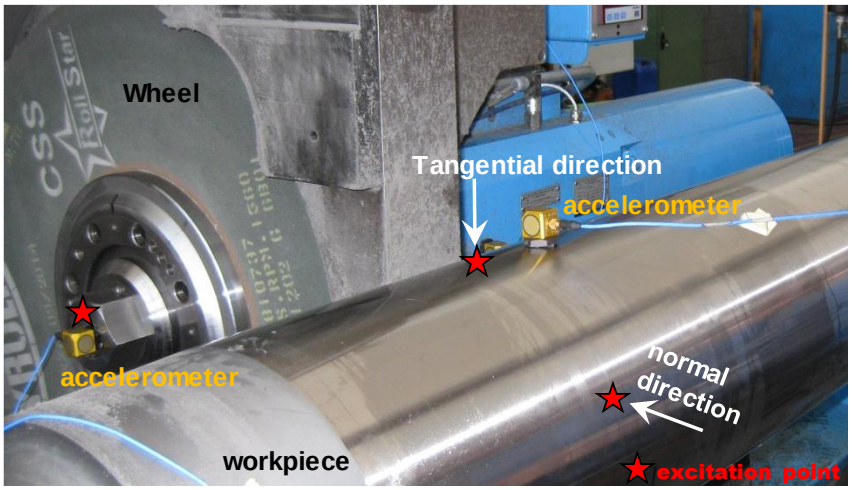

Figure 3. Setup for open-loop FRF measurement

The excitations were exerted at cylinder surface along normal and tangential direction. Force and acceleration signals were acquired via NI™ USB 9234 Data Acquisition System, with a sampling rate of 4096 Hz. Exponential and Hanning windows have been applied to impulsive force and acceleration signals respectively. As acceleration measurements were expected to be affected by parasitic environmental vibration, the FRFs were computed via *H1* estimator [29], which minimizes the error due to output noise. Even if the excitation point in normal direction does not coincide with the measuring point, due to the extreme rigidity of the cylinder portion in between, the corresponding FRF can be considered co-located, as no decoupling eigenmodes are evident — as a matter of fact, the FRFs do not show any resonance beyond 400 Hz. The wheel carriage (Z-axis) was positioned in the middle of the stroke (about 3000 mm), that is in the middle of the cylinder.

Regarding wheel tap testing, to avoid complex excitation in tangential direction on the wheel boundary and accelerometer placement on the abrasive material, the exciting force and corresponding response have been injected and measured at wheel hub. Wheel body compliance is therefore not represented in the measure. As literature unanimously claims that wheel stiffness plays an important role in determining grinding dynamics [30], its effect was estimated by adding a proper static compliance to h_{wn_wn}, i.e. the co-located FRF at wheel boundary, in normal direction.

The stiffness value was estimated via FEM, taking into account the dimension and the material of the wheel, which is a Tyrolit™ 47ACI202 with a nominal diameter of 600 mm and a width of 50 mm. The Young module of the wheel was estimated by matching the first 3 natural frequencies measured via tap testing, in free-free conditions, with the corresponding frequencies computed by the FEM for the first 3 mode shapes. Then, wheel was modelled in contact with an infinitely rigid cylinder with a diameter of 250 mm, loaded with a 1 kN radial force and the resulting approach computed (Figure 4). The result is a 524 N/mm stiffness.

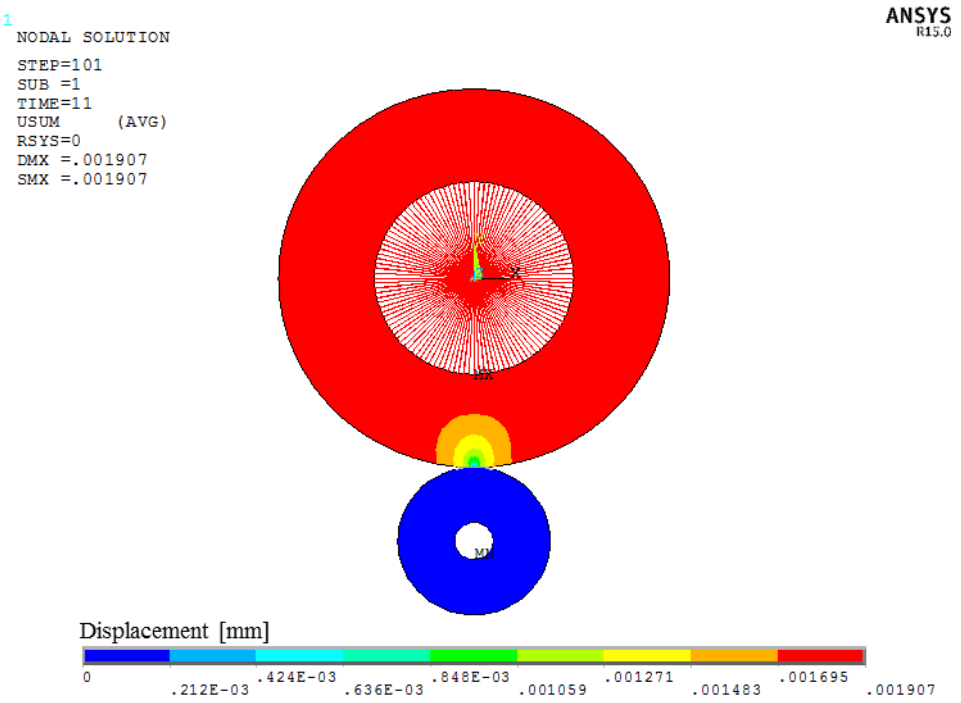

Figure 4. Wheel FEM for stiffness estimation

The elements of the compliance matrix **M** defined in Eq.(12) are depicted in Figure 5.

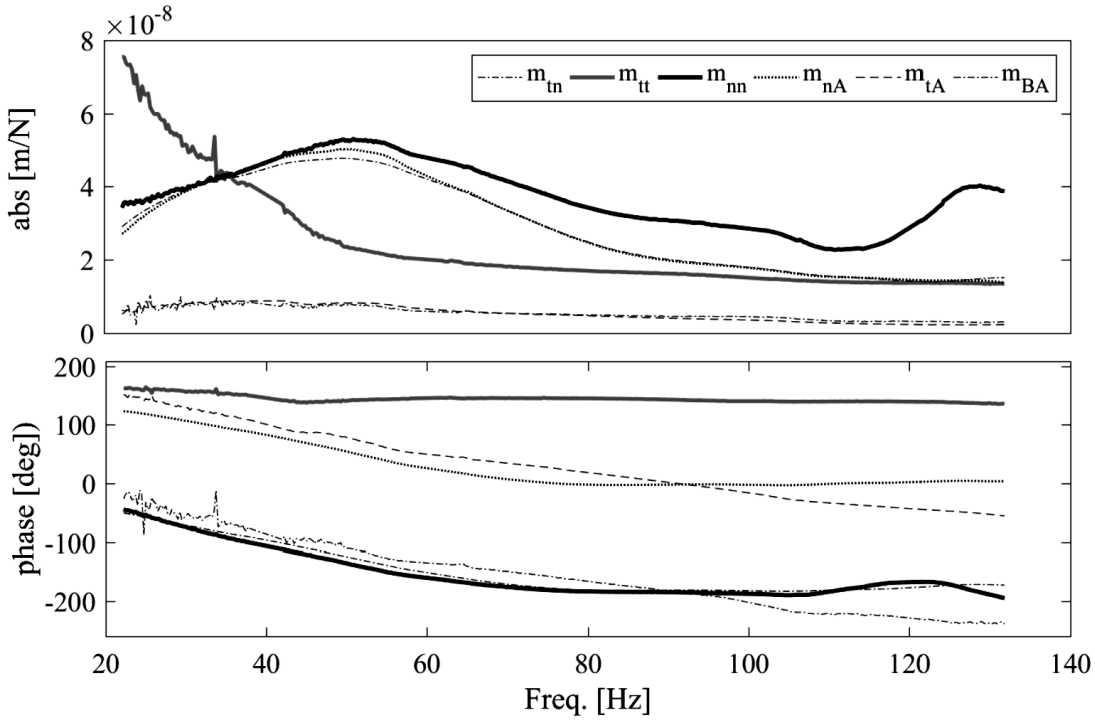

Figure 5. Elements of compliance matrix **M**

5.1.2. Closed-loop FRF measurement and selection

The choice of the proper closed-loop FRF is very important for the quality of process parameters identification. In order to minimize the effect of uncertainties on the Euclidean norm of the solution vector, the input/output pair has to minimize the $\|\bullet\|_2$-condition number of the identification matrix in Eq. (19). Since the condition number reflects the influence of the input excitation on the grinding process, the most suited input/output candidates are the process DoFs: the co-located FRFs — when input and output DoFs are the same — usually entail the maximum displacement amplitude. Then, the condition number of the four systems obtained by posing $A \equiv B \equiv rn, wn, rt, wt$ were compared (see following table): the lowest value corresponds to the DoFs pair $A \equiv B \equiv rn$, because the cylinder is more compliant then the wheel side. Therefore, the closed-loop FRF to be measured during a grinding test is at cylinder side, in normal direction.

Table 1. Condition number evaluation

I/O DoF	Condition number
wt - wt	13.6
rt - rt	9.8
rn - rn	8.8
wn - wn	14.9

Since during a grinding operation the cylinder is rotating, an auxiliary steady surface, constrained to the cylinder surface in normal direction only, was created by propping a steel plate against the cylinder surface, with a preload contact force sufficient to prevent loss of contact under tapping and process forces (Figure 6). Both measuring point (accelerometer) and excitation point are on the metal plate. In order to be sure to hit and measure on the contact line, minimizing excitations of plate eigenmodes, a narrow metal stripe was correspondently welded to the plate (Figure 6); a thin Teflon™ film was glued on the plate on the side facing the cylinder to decrease sliding friction, without adding a significant compliance.

It should be pointed out that the theoretical degree of freedom pertaining the closed-loop FRF should correspond to normal direction at contact point between wheel and cylinder that it is located at the opposite side of actual point. Nevertheless, whereas the cylinder is rather stiff and massive, a local eigenmode decoupling the dynamics of the actual measurement point and the theoretical one is negligible and the 2 points can be confused with each other.

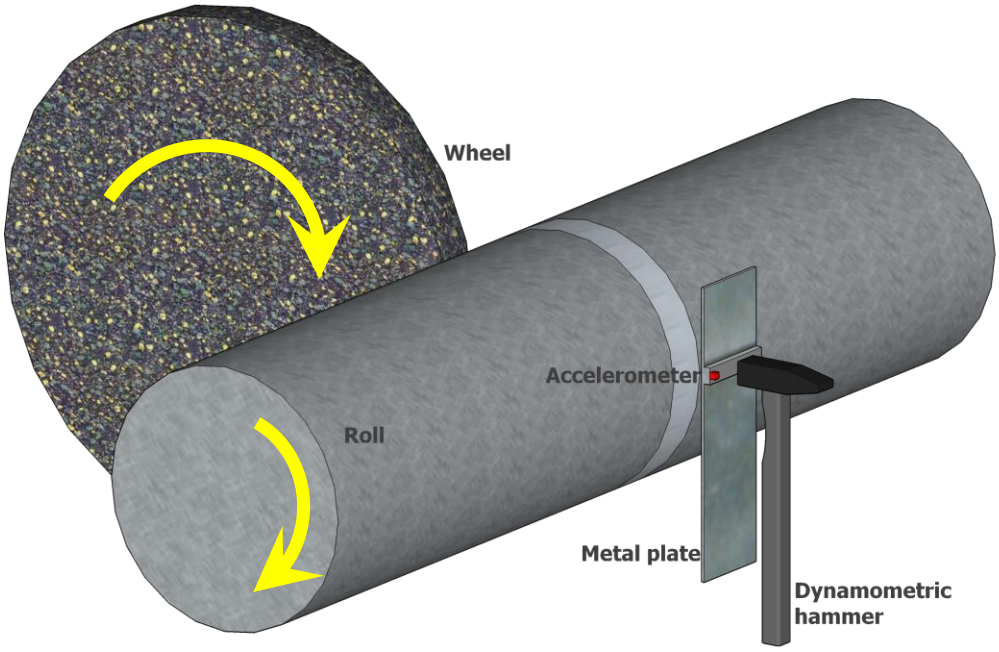

Figure 6. Setup for closed-loop FRF measurement. The metal plate is fixed on the machine structure

The plunge grinding operation executed during closed-loop FRF measurement is described in Table 2. In order to guarantee the coincidence between actual and nominal infeed value, the measurement was executed after a proper dwell time, when the spindle power reached the steady state.

Vs [m/s]	Vw [m/s]	Infeed vel. [mm/s]
41.6	0.737	0.003

Table 2. Grinding parameters for in-process tap-testing

Given the cylinder diameter and the selected infeed velocity, the infeed for turn a, required to compute process matrices $\mathbf{K}_g$ and $\mathbf{K}_{gd}$, is:

$$a = \frac{\dot{a}}{V_w} D_w \pi = 0.003 \text{ mm} \tag{20}$$

The measured closed-loop FRF is depicted in Figure 7, that shows also the coherence, indicating an acceptable linear correlation between input force and output acceleration.

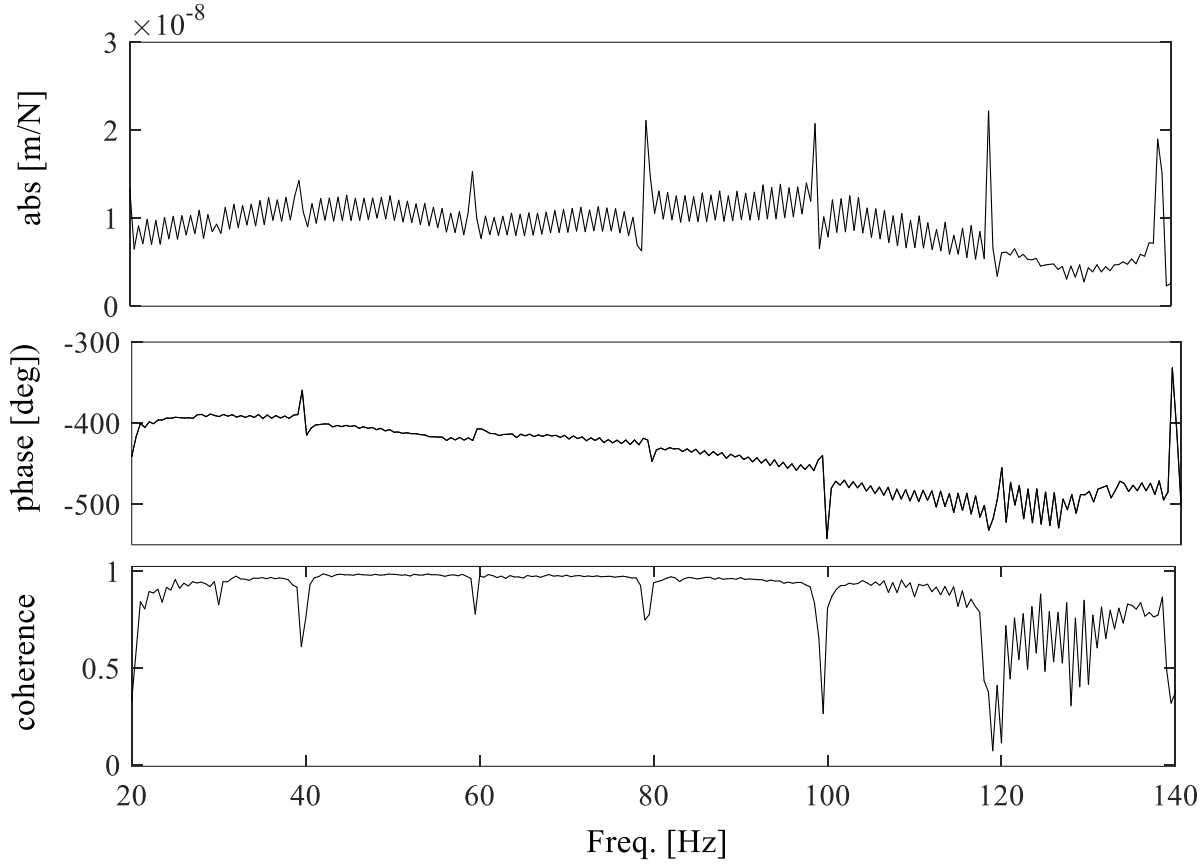

Figure 7. Closed-loop (in-process) FRF

The closed-loop FRF magnitude and phase exhibit a sawed gait due to the periodic disturbances produced by wheel and roll rotation. While the effect of roll rotation (a peak each 1 Hz, in this case) is limited in amplitude, the disturbance ascribable to wheel rotation (a peak every 22 Hz) is rather disruptive, as clearly shown by the corresponding coherence tumbles. Such periodic disturbances are not represented in the adopted machine model and therefore should not be included in the fitting data: for this reason, a 4 Hz interval around each of these latter peaks has been excluded by the identification procedure.

5.1.3. Parameters identification in frequency domain

Now, it is possible to solve the system of Eq.(17) for k_t and k_n. The selected frequency range, i.e. (20÷120 Hz), corresponds to an acceptable coherence of the FRF and a significant amplitude, necessary to get a good numerical conditioning and a limited variance of the estimated parameters (see Figure 7). It yields:

$$k_t = 28.6 \text{ J/mm}^3; \quad k_n = 56.0 \text{ J/mm}^3 \tag{21}$$

Theoretical closed-loop FRF, computed exploiting the identified parameters, is plotted against its experimental counterpart, together with the corresponding open-loop FRF in Figure 8, to assess fitting quality.

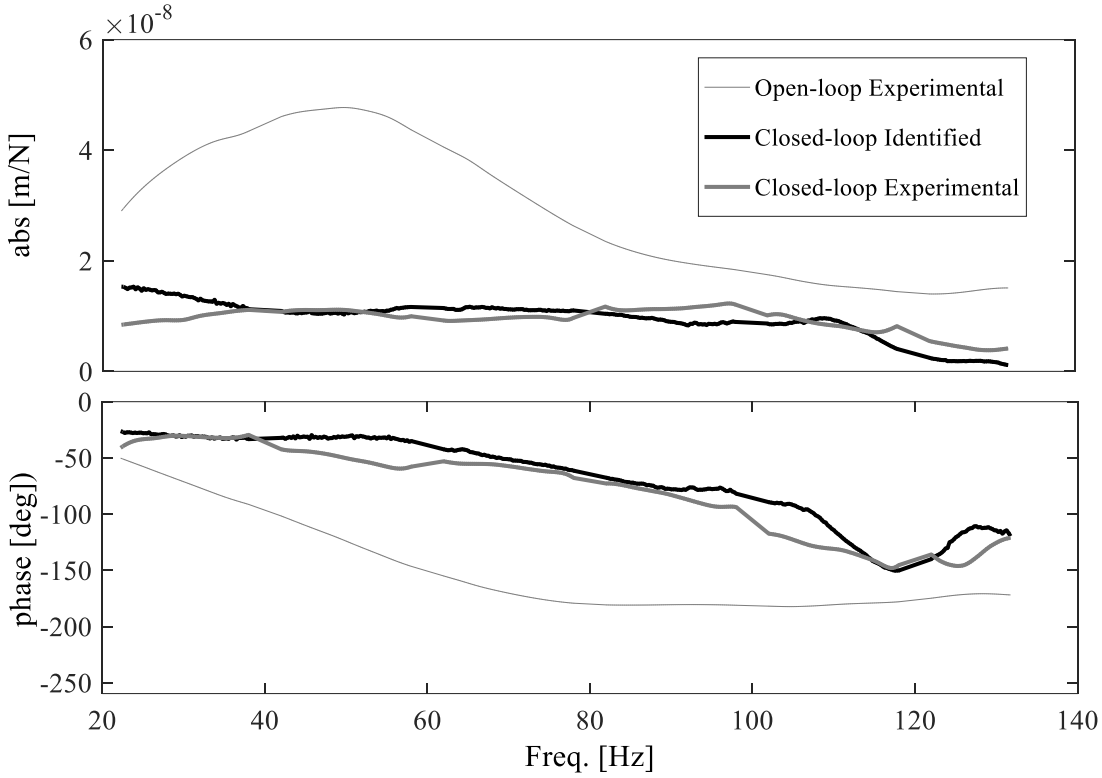

Figure 8 . Closed-loop fitting

The square root of the residual variance over the considered frequency range is equal to 6.7e-9 m/N and the 2σ intervals for the identified parameters, corresponding to a confidence level of 95%, are:

$$2\sigma_{k_t} = 8.5 \text{ J/mm}^3; \quad 2\sigma_{k_n} = 1.4 \text{ J/mm}^3 \tag{22}$$

While the confidence interval associated with k_n is rather good, that one associated with k_t reflects a significant lack of observability. This circumstance is ascribable to the weak coupling between dynamic compliance in tangential and normal direction for the machine under investigation, which makes the identification system partially ill conditioned — as pointed out at the end of par. 3.3. Indeed, the most significant eigenmode in the identification frequency range, at 50 Hz, moves the wheel and the roll mostly in radial direction.

5.2. Specific energy identification from power measurement during grinding tests

The proposed identification methodology can be furtherly assessed by comparing the k_t, obtained in the previous paragraph, with its estimation identified from spindle power measurements during grinding tests. Spindle power measurement is rather simple and does not require any special equipment, as its value is provided directly by the motor drive and sent to the machine supervisor system.

The adopted relationship between specific energy and spindle power is:

$$P_s = k_t MRR + P_{s0} \tag{23}$$

where P_s is the overall spindle motor output power and P_{s0} is the spindle power component for a null *MRR* (mainly due to spindle internal friction and wheel rubbing effect).

Grinding tests consisted in traverse grinding passes without overlapping with a fixed wheel speed of 37 m/s and two different roll speeds. The continuous infeed was set automatically by the machine, having imposed a reference wheel spindle power through a supplementary position control loop on the infeed axis. Wheel type and roll were the same of the plunge grinding operations executed during closed-loop FRF measurement, so that the specific energy identified with the two approaches must coincide.

For each combination of wheel and roll velocity, six passes were executed. The *MRR* was computed multiplying the roll velocity by the grinding width — equal to wheel width, i.e. 50 mm — and the average actual infeed, calculated by measuring roll diameter exploiting a caliper integrated in the machine, before and after the 6 grinding passes.

Table 3 resumes the grinding tests variable parameters with the resulting *MRR* and the measured wheel power.

***Vw* [m/s]**	***a* [mm]**	***MRR* [mm^3/s]**	***Wheel power* [W]**
0.980	0.00144	**70.4**	**5340.8**
0.490	0.00345	**84.6**	**5110.3**
0.490	0.00320	**78.7**	**5088.3**
0.980	0.00123	**61.9**	**4965.2**
0.490	0.00070	**17.2**	**3585.6**
0.490	0.00148	**36.3**	**3488.6**
0.490	0.00120	**27.4**	**3327.9**
0.490	0.00130	**31.6**	**3258.0**
0.490	0.00002	**0.6**	**3211.6**

Table 3. Grinding parameters for in-process tap-testing

Since Eq. (18) must hold for each row of Table 3, an over-determined linear equations system in k_t and P_{s0} is solved in LS sense, yielding:

$$\bar{k}_t = 29.24 \text{ J/mm}^3,\ \sigma_{k_t} = 9.33 \text{ J/mm}^3; \qquad \bar{P}_{s0} = 2824.3 \text{ W},\ \sigma_{P_{s0}} = 496.6 \text{ W} \tag{24}$$

Figure 9 gives a graphical representation of the quality of the fitting. Both k_t nominal value and the 95% confidence interval are very close to those obtained according to the sub-structuring procedure described in the previous paragraph, confirming the validity of the proposed dynamic model.

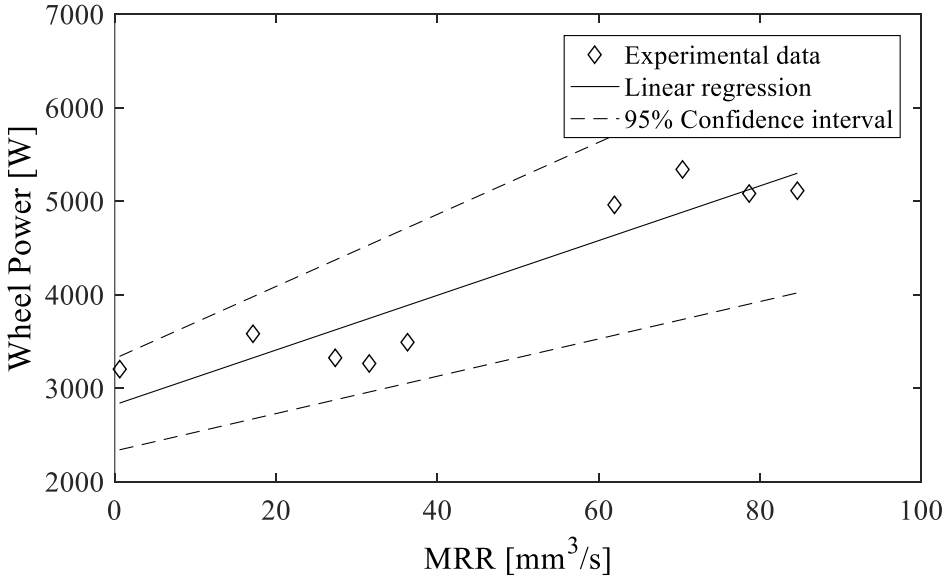

Figure 9. Specific energy k_t identified via power measurements and by sub-structuring.

5.3. Sensitivity analysis

The identification procedure is based on a linearization of the force model of Eq. (1) around the nominal infeed. When vibration occurs, the actual infeed differs from the nominal one; thus, a sensitivity analysis was carried out to evaluate the impact of this approximation on the identification result.

The k_n and k_t identification was repeated considering several values of infeed, spanning an interval of -/+ 10% of the nominal value. The results are reported in Figure 10.

It can be noted that k_t coefficient exhibits the largest variation — around 17 % — of the nominal value: similar uncertainty is reported in the literature [31].

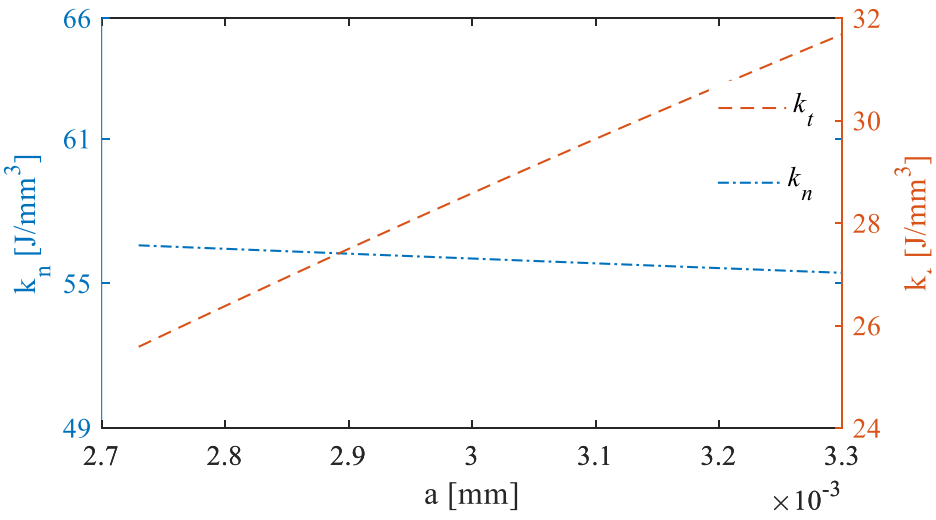

Figure 10. Sensitivity analysis of force model linearization

6. Discussion and Conclusions

A force model describing machine-process interaction in cylindrical grinding was proposed. It is based on two parameters, i.e. grinding specific energy and grinding stiffness, and models the cutting forces in both tangential and normal directions.

The presented methodology for parameters identification — that does not require direct cutting force measurements — is based on the effect that the process has on roll dynamic compliance in normal direction. The model predicts how the dynamic compliance measured at rest (i.e. *out-of-process*) changes when the process is active (i.e. *in-process*).

The proposed identification procedure requires first a dynamic compliance measurement (via tap-testing) at wheel and workpiece in rest condition for both tangential and normal directions. Then an in-process dynamic compliance is measured at cylinder side in normal direction, by means of the developed original setup.

The model well predict the in-process dynamic behavior and provides an estimation of the grinding stiffness in both tangential and normal direction — or, equivalently, the ratio between tangential and normal grinding force components. Due to the poor coupling showed by the examined machine between normal and tangential dynamics of wheel and cylinder for the targeted frequency range, the identification of grinding specific energy resulted more uncertain than the normal force coefficient. The specific energy was identified also exploiting wheel spindle power measurements in standard grinding tests. The comparison of the two identification methodologies — limited to the sole specific energy — confirmed the good performance provided by the proposed method based on tap testing and frequency domain fitting.

The proposed model properly describes the dynamic interaction between grinding process and machine, including the dynamic coupling between tangential and normal directions. Moreover, the original calibration procedure, based on in-process and out-of-process tap testing measurements, allows the exploitability of the model even when the grinding force measurements are unpractical, like in case of large roll grinders. Then, the calibrated model can be effectively exploited in advanced model-based control schemes for grinding chatter avoidance as implemented by the authors in [32]. Future works will be carried out to furtherly improve the technique for in-process FRF measurements, trying to attenuate the disturbances induced by wheel and roll rotation during grinding.

Acknowledgement

This work was supported by the Italian Ministry of Economic Development, in the framework of MICHELANGELO project [Industria 2015, D.M. 05/03/2008].

References

[1]. W.B. Rowe, Principles of Modern Grinding Technology, 2014. doi:10.1016/B978-0-323-24271-4.00017-8.

[2]. E. Brinksmeier, J.C. Aurich, E. Govekar, C. Heinzel, H.-W. Hoffmeister, F. Klocke, J. Peters, R. Rentsch, D.J. Stephenson, E. Uhlmann, Advances in Modeling and Simulation of Grinding Processes, CIRP Ann. - Manuf. Technol. 55 (2006) 667–696. doi:10.1016/j.cirp.2006.10.003.

[3]. I.D Marinescu et al., Handbook of Machining with Grinding Wheels, ed.1, CRC Press, Taylor and Francis Group, 2006, ISBN-10: 1574446711.

[4]. I. Inasaki, B. Karpuschewski, H.-S. Lee, Grinding Chatter – Origin and Suppression, CIRP Ann. - Manuf. Technol. 50 (2001) 515–534. doi:10.1016/S0007-8506(07)62992-8.

[5]. X. Chen, W.B. Rowe, Analysis and simulation of the grinding process. Part II: Mechanics of grinding, Int. J. Mach. Tools Manuf. 36 (1996) 883-896. doi:10.1016/0890-6955(96)00117-4.

[6]. M. Leonesio, P. Parenti, A. Cassinari, G. Bianchi, Force-field instability in surface grinding, Int. J. Adv. Manuf. Technol. (2014). doi:10.1007/s00170-014-5725-7.

[7]. T.L. Schmitz, R.R. Donalson, Predicting high-speed machining dynamics by substructure analysis, CIRP Ann - Manuf Technol, 49 (2000), pp. 303–308.

[8]. S.S. Park, Y.Altintas, M.Movahhedy, Receptance coupling for end mills, Int. J. Mach. Tools Manuf. 43 (2003) 889–896.

[9]. K. Ahmadi, H. Ahmadian, Modelling machine tool dynamics using a distributed parameter tool-holder joint interface, Int. J. Mach. Tools Manuf. 47 (2007) 1916–1928. doi:10.1016/j.ijmachtools.2007.03.004.

[10]. S. Filiz, C.H. Cheng, K.B. Powell, T.L. Schmitz, O.B. Ozdoganlar, An improved tool-holder model for RCSA tool-point frequency response prediction, Precis. Eng. 33 (2009) 26–36. doi:10.1016/j.precisioneng.2008.03.003.

[11]. B. a. Mascardelli, S.S. Park, T. Freiheit, Substructure Coupling of Microend Mills to Aid in the Suppression of Chatter, J. Manuf. Sci. Eng. 130 (2008) 11010. doi:10.1115/1.2816104.

[12]. M.R. Movahhedy, J.M. Gerami, Prediction of spindle dynamics in milling by sub-structure coupling, 46 (2006) 243–251. doi:10.1016/j.ijmachtools.2005.05.026.

[13]. S.S. Park, J. Chae, Joint identification of modular tools using a novel receptance coupling method, Int. J. Adv. Manuf. Technol. 35 (2008) 1251–1262. doi:10.1007/s00170-006-0826-6.

[14]. Y. Ren, C.F. Beards, Identification of joint properties of a structure using FRF data, J. Sound Vib. 186 (1995) 567–587. doi:10.1006/jsvi.1995.0469.

[15]. O. Özşahin, A. Ertürk, H.N. Özgüven, E. Budak, A closed-form approach for identification of dynamical contact parameters in spindle-holder-tool assemblies, Int. J. Mach. Tools Manuf. 49 (2009) 25–35. doi:10.1016/j.ijmachtools.2008.08.007.

[16]. J.F.G. Oliveira, T.V. Franca, J.P. Wang, Experimental analysis of wheel/workpiece dynamic interactions in grinding, CIRP Annals - Manufacturing Technology, 57 (2008) 329–332

[17]. H. Li, Y.C. Shin, A study on chatter boundaries of cylindrical plunge grinding with process condition-dependent dynamics, Int. J. Mach. Tools Manuf. 47 (2007) 1563–1572. doi:10.1016/j.ijmachtools.2006.11.009.

[18]. B. Zhang, J. Wang, F. Yang, Z. Zhu, The effect of machine stiffness on grinding of silicon nitride, Int. J. Mach. Tools Manuf. 39 (1999) 1263–1283.

[19]. P. Parenti, M. Leonesio, A. Cassinari, G. Bianchi, M. Monno, A model-based approach for online estimation of surface waviness in roll grinding, Int. J. Adv. Manuf. Technol. (2015). doi:10.1007/s00170-015-6864-1.

[20]. W.B. Rowe, X. Chen, Characterization of the size effect in grinding and the sliced bread analogy, Int. J. Prod. Res. 35 (1997) 887–899. doi:10.1080/002075497195768.

[21]. H.A. Razavi, T.R. Kurfess, S. Danyluk, Force control grinding of gamma titanium aluminide, Int. J. Mach. Tools Manuf. 43-2 (2003) 185–91.

[22]. J.C. Ramos, J. Vinolas, F.J. Nieto, Simplified methodology to determine the cutting stiffness and the contact stiffness in the plunge grinding process, Int. J. Mach. Tools Manuf. 41 (2001) 33–49. doi:10.1016/S0890-6955(00)00062-6.

[23]. A.W. Moerlein, E.R. Marsh, T.R.S. Deakyne, R.R. Vallance, In-process force measurement for diameter control in precision cylindrical grinding, Int. J. Adv. Manuf. Technol. 42 (2009) 93–101. doi:10.1007/s00170-008-1584-4.

[24]. M. Leonesio, P. Parenti, A. Cassinari, G. Bianchi, M. Monno, A time-domain surface grinding model for dynamic simulation, in: Procedia CIRP, 2012: pp. 166–171. doi: 10.1016/j.procir.2012.10.030

[25]. H.C. Chang, K.H. Chen, J. Wang, C.Y. Wu, Method for evaluating grinding parameters of grinding wheel, European Patent Application, EP Pat. EP2159002A1 (2010).

[26]. H.E. Jenkins, T.R. Kurfess, Adaptive pole-zero cancellation in grinding force control, IEEE Trans. Control Syst. Technol. 7 (1999) 363–370. doi:10.1109/87.761056.

[27]. I. Inasaki, S. Yonetsu, Forced Vibrations during Surface Grinding, Bullettin of JSME. 12-50 (1969)

[28]. J.H. Gordis, R.L. Bielawa, W.G. Flannelly. A general theory for frequency domain structural synthesis. J. Sound Vib. 150 (1991), 139–158.

[29]. D.j. Ewins, Modal Testing, Theory, Practice, and Application (2nd Edition), RSP Edition, Baldock, England (2000), ISBN-13: 978-0863802188.

[30]. R. Baylis, B. Stone, The effect of grinding wheel flexibility on chatter. CIRP Annals-Manufacturing Technology, 38-1 (1989) 307–310.

[31]. V.K. Mishra, K. Salonitis, Empirical estimation of grinding specific forces and energy based on a modified werner grinding model, Procedia CIRP. 8 (2013) 287–292. doi:10.1016/j.procir.2013.06.104.

[32]. P. Parenti, M. Leonesio, G. Bianchi, Model-based adaptive process control for surface finish improvement in traverse grinding, Mechatronics. (2016). doi:10.1016/j.mechatronics.2016.04.001.